CHEMISTRY OF MATERIALS
Article

Chem. Mater. **2010,** *22,* 5251–5257 5251
DOI:10.1021/cm101262s

Influence of Size, Shape, and Surface Coating on the Stability of Aqueous Suspensions of CdSe Nanoparticles

Martin J. Mulvihill,[†,‡] Susan E. Habas,[†] Ilan Jen-La Plante,[†] Jiamin Wan,[‡] and Taleb Mokari*[,†,§]

[†]*Molecular Foundry at Lawrence Berkeley National Laboratory, Berkeley California 94720, and* [‡]*Earth Science Division at Lawrence Berkeley National Laboratory, Berkeley, California 94720.* [§]*Current address: Department of Chemistry, Ben Gurion University of the Negev, Beer Sheva, Israel.*

Received May 5, 2010. Revised Manuscript Received August 3, 2010

In response to the rapid development and emerging commercialization of nanoparticles, fundamental studies concerning the fate of nanoparticles in the environment are needed. Precise control over the nanoparticle size, shape, and surface coating of cadmium selenide particles modified with thiolate ligands has been used to analyze the effects of nanoparticle design on their stability in aqueous environments. Nanoparticle stability was quantified using the concept of critical coagulation concentration (CCC) in solutions of sodium chloride. These investigations characterized the instability of the ligand coatings, which varied directly with chain length of the capping ligands. The stability of the ligand coatings were characterized as a function of time, pH, and ionic strength. Ligand dissociation has been shown to be a primary mechanism for nanoparticle aggregation when short-chain (C_2-C_6) ligands are used in the ligand shell. Stable nanoparticle suspensions prepared with long chain ligands (C_{11}) were used to characterize nanoparticle stability as a function of size and shape. A linear relationship between particle surface area and the CCC was discovered and was found to be independent of nanoparticle shape. Quantitative analysis of nanoparticle size, shape, and surface coating demonstrated the importance of ligand stability and particle surface area for the prediction of nanoparticle stability.

Introduction

The development of cadmium selenide nanomaterials has a 20 year history, focusing extensively on chemical control over size and shape.[1−6] The sustained interest in these materials has been a result of their size-dependent optical properties,[7−10] which make CdSe nanomaterials attractive for biological labeling[11,12] and solar energy conversion applications.[13,14] The resulting commercial potential for these materials has led government agencies to identify semiconductor quantum dots, including CdSe, as a class of nanoparticles whose health and environmental risks must be quantified.[15−17]

Understanding nanoparticle stability within the environment is an essential first step for the evaluation of risks.[18−22] Nanoparticle transport through the environment will take place through waterways and aquifers.[21−26] Hence, studies concerning the stability of nanoparticles in aqueous

*To whom correspondence should be addressed. E-mail: mokari@bgu.ac.il.

(1) Brennan, J. G.; Siegrist, T.; Carroll, P. J.; Stuczynski, S. M.; Reynders, P.; Brus, L. E.; Steigerwald, M. L. *Chem. Mater.* **1990**, *2*, 403–409.
(2) Mokari, T.; Banin, U. *Chem. Mater.* **2003**, *15*, 3955–3960.
(3) Murray, C. B.; Norris, D. J.; Bawendi, M. G. *J. Am. Chem. Soc.* **1993**, *115*, 8706–8715.
(4) Peng, X. G.; Manna, L.; Yang, W. D.; Wickham, J.; Scher, E.; Kadavanich, A.; Alivisatos, A. P. *Nature* **2000**, *404*, 59–61.
(5) Peng, Z. A.; Peng, X. G. *J. Am. Chem. Soc.* **2002**, *124*, 3343–3353.
(6) Yin, Y.; Alivisatos, A. P. *Nature* **2005**, *437*, 664–670.
(7) Brus, L. *J. Phys. Chem.* **1986**, *90*, 2555–2560.
(8) Wang, Y.; Herron, N. *J. Phys. Chem.* **1991**, *95*, 525–532.
(9) Alivisatos, A. P. *Science* **1996**, *271*, 933–937.
(10) Yu, W. W.; Qu, L. H.; Guo, W. Z.; Peng, X. G. *Chem. Mater.* **2003**, *15*, 2854–2860.
(11) Bruchez, M.; Moronne, M.; Gin, P.; Weiss, S.; Alivisatos, A. P. *Science* **1998**, *281*, 2013–2016.
(12) Han, M. Y.; Gao, X. H.; Su, J. Z.; Nie, S. *Nat. Biotechnol.* **2001**, *19*, 631–635.
(13) Gur, I.; Fromer, N. A.; Geier, M. L.; Alivisatos, A. P. *Science* **2005**, *310*, 462–465.
(14) Huynh, W. U.; Dittmer, J. J.; Alivisatos, A. P. *Science* **2002**, *295*, 2425–2427.
(15) Committee for Review of the Federal Strategy to Address Environmental, Health, and Safety Research Needs for Engineered Nanoscale Materials, Committee on Toxicology, National Research Council. *Review of Federal Strategy for Nanotechnology-Related Environmental, Health, and Safety Research*; The National Academy of Science: Washington, DC, 2009.
(16) Godwin, H. A.; Chopra, K.; Bradley, K. A.; Cohen, Y.; Harthorn, B. H.; Hoek, E. M. V.; Holden, P.; Keller, A. A.; Lenihan, H. S.; Nisbet, R. M.; Nel, A. E. *Environ. Sci. Technol.* **2009**, *43*, 6453–6457.
(17) Wiesner, M. R.; Lowry, G. V.; Jones, K. L.; Hochella, M. F.; Di Giulio, R. T.; Casman, E.; Bernhardt, E. S. *Environ. Sci. Technol.* **2009**, *43*, 6458–6462.
(18) Dhawan, A.; Taurozzi, J. S.; Pandey, A. K.; Shan, W. Q.; Miller, S. M.; Hashsham, S. A.; Tarabara, V. V. *Environ. Sci. Technol.* **2006**, *40*, 7394–7401.
(19) Franklin, N. M.; Rogers, N. J.; Apte, S. C.; Bately, G. E.; Gadd, G. E.; Casey, P. S. *Environ. Sci. Technol.* **2007**, *41*, 8484–8490.
(20) Handy, R. D.; von der Kammer, F.; Lead, J. R.; Hassellov, M.; Owen, R.; Crane, M. *Ecotoxicology* **2008**, *17*, 287–314.
(21) Nowack, B.; Bucheli, T. D. *Environ. Pollut.* **2007**, *150*, 5–22.
(22) Simonet, B. M.; Valcarcel, M. *Anal. Bioanal. Chem.* **2009**, *393*, 17–21.
(23) Brant, J.; Lecoanet, H.; Wiesner, M. R. *J. Nanopart. Res.* **2005**, *7*, 545–553.
(24) Hassellov, M.; Readman, J. W.; Ranville, J. F.; Tiede, K. *Ecotoxicology* **2008**, *17*, 344–361.

Published on Web 08/17/2010

systems are essential for the development of predictive fate and transport models.[17,27] Furthermore, the stability of nanoparticles has been shown to influence their toxicity,[28−30] increasing the need to understand the behavior of nanoparticle suspensions. In general, nanoparticle stability is mediated by chemical and physical properties including size,[31,32] shape, material composition,[19,27,33,34] and surface coating.[30,31,35−38] This article highlights the role of ligand design, as well as nanoparticle shape, on the stability of nanoparticle suspensions.

Preliminary studies on the effects ligands have on CdSe nanocrystal stability have shown the important role that both pH and photochemistry play in quantum dot stability.[31,39] These studies used chemical methods to characterize the degradation of quantum dots. Using UV−vis, Aldana et al. were able to characterize the relative stability of various size CdSe nanoparticles with short-chain thiols. They concluded that smaller particles were stable over a wider pH range because of stronger interactions between the nanoparticles and the capping agents.[31] These results, along with earlier work looking at other hydrophobic thiols in organic solutions,[39] pointed toward the primary importance of the nanoparticle/ligand interaction in dictating the stability of nanoparticle suspensions.

Our work has focused on the kinetics of aggregation and found that the kinetic stability of ligand shells is affected by secondary interactions between ligands. These interactions were studied by varying the number of carbon atoms present between the thiol and pendant carboxylic acid. Our results demonstrated that longer ligands formed significantly more stable suspensions over a wide range of salt concentrations. This has been explained using kinetic models, rather than the thermodynamic ligand/particle interaction that was previously characterized.[31,37,39] This allowed the preparation of various particles morphologies which were all kinetically stable. These particles were used to demonstrate a relationship between nanoparticle surface area and nanoparticle stability.

This article has quantified stability using the critical coagulation concentration (CCC) as a metric.[40−42] The initial stages of aggregation have been monitored by dynamic light scattering (DLS), enabling the quantification of kinetic destabilization. Nanoparticle size and morphology were compared using four different CdSe particle samples (with diameters of 4 nm, 6 nm, and 8 nm, and rods of 3 × 24 nm). The influence of the ligand shell composition was studied using thiolate ligands. In particular, the effects of chain length and surface charge were studied as a function of pH, ionic strength, free ligand, and time. All of the particles in this study were synthesized in our laboratory, which enabled us to study these key parameters in a controlled manner.

Experimental Section

The following chemicals were purchased from Sigma-Aldrich and used as received: selenium powder, cadmium oxide, 11-mecaptoundecanoic acid (MUA), 3-mercaptopropionic acid (MPA), 6-mercaptohexanoic acid (MHA), mercaptopropyl alcohol (MPOH), sodium chloride, oleylamine, oleic acid, and octadecene. Dimethylcadmium, trioctylphosphine (TOP, 99%), and tri-*n*-butylphosphine (TBP, 99%) were purchased from Strem. Dimethyl cadmium was used as received and stored inside a N_2 glovebox. Tetradecylphosphonic acid (TDPA) was purchased from Alfa Aesar. All water used was purified with a Millipore filtration system and had >18 MΩ resistivity.

A Malvern Zetasizer Nano (ZEN3600) with a 633 nm excitation source was employed for both the DLS and zeta-potential measurements. UV−vis spectra were obtained with a Shimadzu UV-3101 PC spectrophotometer. ATR-FTIR was preformed on a Perkin-Elmer Spectrum One FTIR with a HATR attachment. H^1-NMR spectra were collected using a 500 MHz Bruker instrument. NMR measurements were conducted in D_2O (from Cambridge isotope lab) unless otherwise noted. TEM measurements were preformed on a 200 KeV Hitachi TEM.

Dynamic Light Scattering Measurements. DLS and zeta-potential measurements were obtained using a Malvern Zetasizer nano(zs). Hydrodynamic radii (Z-Average) were calculated from the correlation function using software provided by Malvern. All measurements were performed in buffered solutions (2.5 mM carbonate buffer pH = 10) with the same initial starting concentration of particles, unless otherwise noted. All experiments were run with a 7×10^{-7} M particle concentration which corresponds to a number density of 4×10^{20} m^{-3}. The concentration of CdSe particles was determined using UV−vis spectroscopy and the reported values for the extinction coefficients,[10] and then verified by ICP-AES. To measure the aggregation rates, readings were taken every 30 s for 15 min, and rates were then determined from the linear portion of the curve. Examples of the raw data can be found in Supporting Information (Figure S1).

Electrophoretic mobility measurements were carried out in the same particle solutions using the Malvern Zetasizer nano(zs) with dip cell attachment. Electrophoretic motilities were converted to zeta-potentials using Henry's function and the Smoluchowski approximation for aqueous electrolytes. Examples

(25) Mylon, S. E.; Chen, K. L.; Elimelech, M. *Langmuir* **2004**, *20*, 9000–9006.
(26) Quevedo, I. R.; Tufenkji, N. *Environ. Sci. Technol.* **2009**, *43*, 3176–3182.
(27) Puzyn, T.; Leszczynska, D.; Leszczynska, J. *Small* **2009**, *5*, 2494–2509.
(28) Lewinski, N.; Colvin, V.; Drezek, R. *Small* **2008**, *4*, 26–49.
(29) Nam, J.; Won, N.; Jin, H.; Chung, H.; Kim, S. *J. Am. Chem. Soc.* **2009**, *131*, 13639–13645.
(30) Ojea-Jimenez, I.; Puntes, V. *J. Am. Chem. Soc.* **2009**, *131*, 13320–13327.
(31) Aldana, J.; Lavelle, N.; Wang, Y. J.; Peng, X. G. *J. Am. Chem. Soc.* **2005**, *127*, 2496–2504.
(32) Liu, J.; Aruguete, D.; Murayama, M., M. F. H., Jr. *Environ. Sci. Technol.* **2009**, *43*, 8178–8183.
(33) Adams, L. K.; Lyon, D. Y.; Alvarez, P. J. J. *Water Res.* **2006**, *40*, 3527–3532.
(34) Kirchner, C.; Liedl, T.; Kudera, S.; Pellegrino, T.; Javier, A. M.; Gaub, H. E.; Stolzle, S.; Fertig, N.; Parak, W. J. *Nano Lett.* **2005**, *5*, 331–338.
(35) Dederichs, T.; Moller, M.; Weichold, O. *Langmuir* **2009**, *25*, 10501–10506.
(36) Faure, A. C.; Dufort, S.; Josserand, V.; Perriat, P.; Coll, J. L.; Roux, S.; Tillement, O. *Small* **2009**, *5*, 2565–2575.
(37) Ji, X. H.; Copenhaver, D.; Sichmeller, C.; Peng, X. G. *J. Am. Chem. Soc.* **2008**, *130*, 5726–5735.
(38) Schrier, J.; Wang, L. W. *J. Phys. Chem. B* **2006**, *110*, 11982–11985.
(39) Aldana, J.; Wang, Y. A.; Peng, X. G. *J. Am. Chem. Soc.* **2001**, *123*, 8844–8850.
(40) Chen, K. L.; Mylon, S. E.; Elimelech, M. *Environ. Sci. Technol.* **2006**, *40*, 1516–1523.
(41) Gregory, J. *J. Colloid Interface Sci.* **1973**, *42*, 448–456.
(42) Gregory, J. *Adv. Colloid Interface* **2009**, *147−48*, 109–123.

of typical zeta-potential distributions for each nanoparticle type can be found in Supporting Information (Figure S2).

Critical Coagulation Concentration Determination. Dynamic light scattering (DLS) is an effective way to characterize the rate of aggregation for monodisperse colloidal solutions.[40,42−44] Initially, aggregation is dominated by bimolecular collisions, with a rate constant, k_{11}, and activation energy, E_a. The rate constant is a function of temperature, pH, and ionic strength. In particular, increasing the ionic strength decreases the electrostatic repulsion between particles, increasing k_{11}. At a critical salt concentration, the barrier for particle sticking decreases sufficiently and aggregation becomes diffusion limited. The diffusion limited rate constant is $(k_{11})_{diff}$. The concentration of salt at which k_{11} equals $(k_{11})_{\mathrm{diff}}$ is defined as the critical coagulation concentration. The CCC can be used to compare the relative stability of various particle morphologies as a function of ionic strength.[40,41]

The second order rate law for the two-body interaction between isolated colloids to form a dimer, as determined from previous experiments,[25,41,43] can be expressed as eq 1, where N_1 is the concentration of isolated particles as a function of t, and N_0 is the initial concentration of particles.

$$\left(\frac{dN_1}{dt}\right)_{t\to 0} = -k_{11}N_0^2 \tag{1}$$

During the early stages of the aggregation, the decrease in the singlet concentration will be dominated by doublet formation. As such, this equation can be expressed in terms of doublet formation whose concentration is denoted N_2 (eq 2).

$$\left(\frac{dN_2}{dt}\right)_{t\to 0} = \frac{1}{2}k_{11}N_0^2 \tag{2}$$

It has been shown that within the Rayleigh−Gans−Debye approximation, where all of the primary scattering particles are small compared with the wavelength of the incident light, the absolute aggregation rate constant, k_{11}, can be determined empirically using time-resolved, fixed-angle dynamic light scattering.[16,40,43] During the initial stages of aggregation, the change in hydrodynamic radius, r_{h} is directly proportional to k_{11} (eq 3).[25,41,43]

$$\left(\frac{dr_h}{dt}\right)_{t\to 0} \propto k_{11}N_0 \tag{3}$$

Consequently, the rate of aggregation can be quantified by identifying the slope for the linear portion on a plot of hydrodynamic radius vs time (see Supporting Information, Figure S1). When the aggregation proceeds beyond the dimer limit $r_{\mathrm{h}} > 1.4r$, the calculated value, $\mathrm{d}r_{\mathrm{h}}/\mathrm{d}t$, no longer represents k_{11}, rather a generic initial rate of aggregation. In this study, initial rates were calculated from the linear portion of the $\mathrm{d}r_{\mathrm{h}}/\mathrm{d}t$ curve and excluded hydrodynamic radii values greater than 1500 nm.

Synthesis of 4.1 nm CdSe Nanoparticles. Small 4.1 nm CdSe particles were synthesized using CdO and TOPSe precursors in a mixture of oleylamine, oleic acid, and octadecene. The synthesis was done in a Symyx automated nanocrystal synthesizer using previously reported procedures.[45,46]

Synthesis of 6 and 8 nm CdSe Nanoparticles. Larger CdSe particles were synthesized using a previously reported procedure.[45] In a typical reaction CdO (0.253 g, 1.79 mmol), oleic acid (1.699 g, 6.01 mmol), oleylamine (6.82 g, 25.50 mmol), and octadecene (42.5 mL) were all added to a three neck flask fitted with a condenser, septa, thermocouple, and a needle. The flask was purged with nitrogen while stirring for 1 h at 100 °C to remove excess moisture. The mixture was then heated to 260 °C until the mixture became clear, indicating the formation of the cadmium−oleate complex. This mixture was then cooled to room temperature while being kept under a positive pressure of nitrogen. Separately, a 1 M solution of selenium in trioctylphosphine (TOPSe) was prepared by adding 0.788 g of selenium powder to 10 mL of TOP inside of a nitrogen glovebox. This mixture was stirred at room temperature until a clear and colorless solution was obtained. The TOPSe solution (3.15 mL) was then mixed with the Cd-oleate solution (49.5 mL) at room temperature under nitrogen in a syringe, attached to a syringe pump. This growth solution was set aside while the seed particles were prepared by heating the remaining 6 mL of Cd-oleate to 260 °C and rapidly injecting 350 μL of TOPSe while vigorously stirring. The solution immediately turned red indicating the nucleation of CdSe particles. The initial reaction was allowed to proceed for 6 min, at which time the syringe pump began to deliver the remaining growth solution (Cd-oleate + TOPSe) at a rate of 0.125 mL/min. This slow addition was continued until all of the growth solution had been added to the reaction mixture. Following the addition of the growth solution, the mixture was cooled to 80 °C, and 50 mL of toluene was added. The crude product was then fractionated with toluene and ethanol to remove excess reactants and achieve a narrow size distribution of 8 nm particles. The same reaction was stopped at 40 min to obtain 6 nm particles.

CdSe Rod Preparation. Nanorods were prepared using the more reactive dimethylcadmium precursor along with a tri-*n*-butylphosphine (TBP)−selenium complex and tetradecylphosphonic acid (TDPA) as the capping agent.[2] The precursor solution was prepared in a nitrogen glovebox and consisted of dimethylcadmium (0.164 g, 1.15 mmol) and selenium powder (0.09 g, 1.15 mmol), both dissolved in TBP (2.8 g, 16.4 mmol). To prepare CdSe rods, TOPO (4 g, 10.3 mmol) and TDPA (0.52 g, 20 mol %) were heated to 360 °C in a three neck flask fitted with a condenser, septa, and thermocouple under a nitrogen atmosphere while stirring. To this mixture, 2 g of the precursor solution was rapidly injected to initiate CdSe growth. This rapid injection caused a decrease in the reaction temperature, and further growth took place at a temperature of 290 °C. After 2 min, more of the growth solution was added at a rate of 0.25 mL/min. Once the addition was complete, the reaction was heated for an additional 30 min before cooling.

Surface Modification of the CdSe Nanoparticles. Surface modification was achieved by a two-phase interfacial exchange method,[47] where nanoparticles suspended in chloroform were transferred to water after ligand exchange at the water/chloroform interface. Washed CdSe nanoparticles were suspended in 5 mL of chloroform, in a 20 mL glass vial. On top of this solution was added a basic degassed aqueous solution of tertbutyl ammonium hydroxide (~50 mM) and a thiol ligand (~10 mM). This solution was stirred until the nanoparticles had transferred from the chloroform to the water layer as indicated by the red color. The water-soluble particles were then decanted and allowed to

(43) Holthoff, H.; Egelhaaf, S. U.; Borkovec, M.; Schurtenberger, P.; Sticher, H. *Langmuir* **1996**, *12*, 5541–5549.
(44) Midmore, B. R. *Colloids Surf.* **1991**, *60*, 291–307.
(45) Yen, B. K. H.; Gunther, A.; Schmidt, M. A.; Jensen, K. F.; Bawendi, M. G. *Angew. Chem., Int. Ed.* **2005**, *44*, 5447–5451.
(46) Chan, E.; Milliron, D. *Nano Lett.* **2010**, *10*, 1874–1885.
(47) Warner, M. G.; Reed, S. M.; Hutchison, J. E. *Chem. Mater.* **2000**, *12*, 3316–3320.

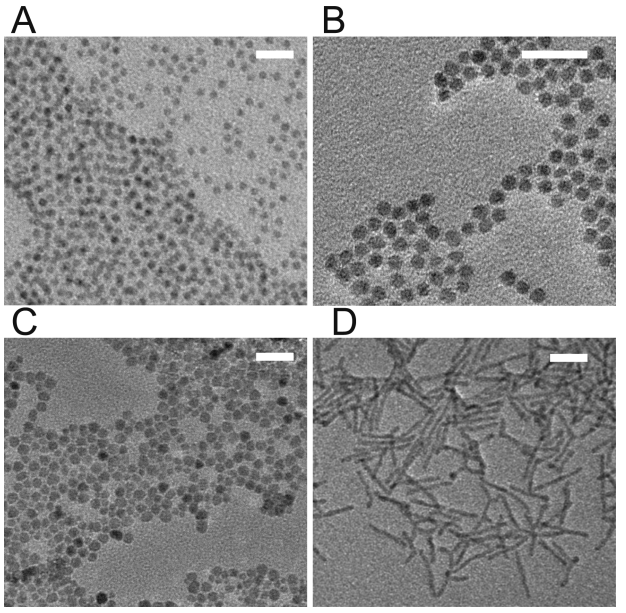

Figure 1. TEM images of each of the nanoparticle starting materials. Scale bars represent 20 nm. (A) CdSe spheres, 4.1 ± 0.4 nm. (B) CdSe spheres, 5.8 ± 0.5 nm. (C) Large CdSe spheres, 7.8 ± 0.5 nm. (D) CdSe rods, 2.9 ± 0.2 nm × 24 ± 3 nm. Corresponding histograms that show nanoparticle size distributions can be found in Supporting Information.

continue the exchange process overnight. Excess ligand was then removed through successive centrifugal filtrations using Amicon Ultra-15 Centrifugal filter tubes with 10,000 MWCO cellulose membrane inserts, which isolate the particles while removing the water and excess ligand. The extent of ligand exchange was followed by NMR, FTIR, and DLS where applicable.

Results and Discussion

Synthesis and Ligand Exchange. CdSe nanoparticles were chosen as a model system for this study because of their unique tunable chemical and physical properties[4] and their associated potential for commercialization. Figure 1 presents TEM images of the CdSe nanoparticles employed in this study. All of the particles were prepared in-house using previously reported procedures. All of the nanoparticle samples maintained less than 10% size variation between particles (Supporting Information, Figure S3).

As made, the CdSe particles were capped with oleylamine, which was displaced in a biphasic ligand exchange reaction to give water-soluble particles capped with 11-mercaptoundecanoic acid (MUA). The extent of the displacement reaction was monitored by NMR (Figure 2). Free and bound ligands were distinguished in NMR by the peak width which showed significant broadening for ligands bound to the surface of nanoparticles.[48,49] Figure 2a shows the as-made particles in chloroform capped with oleylamine. The broad peaks at 1.5 ppm correspond to methylene groups in the oleylamine tail, and the peak at 2.1 ppm corresponds to the methylene group next to the amine.

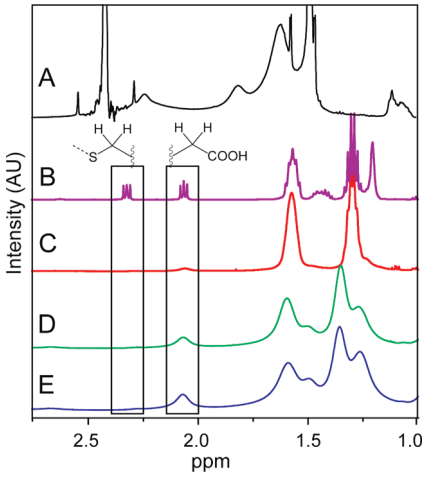

Figure 2. NMR spectra following the exchange and cleaning process of water-soluble CdSe nanoparticles. Starting with (A) oleylamine capped particles, (B) MUA in water is used to displace the amine capping agent. (C) The crude product is then washed repeatedly (D−E) to remove residual MUA from the solution.

Figure 2b provides the spectrum of the water-soluble capping agent MUA. In order to promote solubility of the MUA, a small amount of base was added to the solution. The methylene group alpha to the carboxylic acid appeared as a triplet at 2.1 ppm and served as a good marker for the exchange of oleylamine for MUA. The triplet at 2.3 ppm corresponds to the methylene group next to the thiol. Figure 2c shows the spectrum of the particles following transfer from chloroform to water. After the oleylamine was displaced by MUA, the peak corresponding to the thiol methylene disappeared because of the restricted motion near the surface of the nanoparticle.[37,48,49] Conversely, the carboxylic acid methylene peak at 2.1 ppm broadened and remained present throughout the washing process. The remaining peaks were relatively narrow and correspond to excess MUA in solution. After successive washings to remove excess ligand (spectra 2d-e), broad methylene peaks from 1.0 to 1.5 ppm appeared, and the broad peak at 2.1 indicated the presence of the carboxylic acid moiety. Three key pieces of information were obtained through NMR analysis: (1) oleylamine has been displaced by MUA, (2) MUA bonded through the thiol rather than the carboxylic acid moiety, and (3) excess MUA was removed by repeated washing. Additional evidence of the ligand exchange was provided by ATR-FTIR which clearly shows the presence of carboxylate groups after the ligand exchange reaction (see Supporting Information, Figure S4).

The surface charge on each particle sample was characterized by electrophoretic mobility measurements, which were converted to zeta-potentials using the Smoluchowski approximation (Table 1). These potentials are related to the surface charge density of the underlying particle and can be used to compare the relative surface charge densities of various particles. As seen in Table 1, our exchange method produced similar charge densities on each type of particle. The NMR and zeta-potential measurements indicated that, although the particle samples were different sizes and shapes, these four types of particles all had similar surface chemistry. As a control, nanoparticles were capped with

(48) Owen, J. S.; Park, J.; Trudeau, P. E.; Alivisatos, A. P. *J. Am. Chem. Soc.* **2008**, *130*, 12279–12281.
(49) Woehrle, G. H.; Brown, L. O.; Hutchison, J. E. *J. Am. Chem. Soc.* **2005**, *127*, 2172–2183.

Table 1. Zeta Potentials, as Calculated from Electrophoretic Mobility, for Each Particle Type

size	capping agent	zeta potential (mV)
7.8 nm	MUA	-33 ± 5
2.9 × 24 nm	MUA	-37 ± 3
5.8 nm	MUA	-34 ± 4
4.1 nm	MUA	-35 ± 3
4.1 nm	MHA	-34 ± 5
4.1 nm	MPA	-33 ± 3
4.1 nm	MPOH	0 ± 7

mercaptopropyl alchol (MPOH). Particles capped with this neutral ligand had negligible zeta potentials (0 ± 7). This supports the claim that the surface charges originate from the ligand shell rather than the underlying particle surface.

Influence of Ligand Type. The nanoparticle/ligand interaction has been shown to dictate the size and shape of nanoparticles during the growth process[4,50,51] and has also been determined to affect the stability of nanoparticle suspensions.[31,37,39] To evaluate the nanoparticle/ligand interaction, a series of thiol terminated aliphatic carboxylic acids with varying chain lengths (C_3, C_6, and C_{11}) were investigated. Immediately following the ligand exchange reactions on the 4.1 nm CdSe nanoparticle surfaces, samples made with each of the three capping agents were all shown to have the same zeta-potential (see Table 1). Any differences in the CCC for these samples is therefore a function of the ligand/particle interaction. Ligand coatings based on longer chain ligands are expected to be more stable because of increased van der Waals interactions between neighboring hydrophobic chains.

The role of ligand dissociation in the destabilization of particles suspensions was measured by the aggregation of particles in suspensions with no added salt. Suspensions of particles with each of the ligands in pure water were monitored over the course of 12 h (Figure 3a). These results show that even without added salt the CdSe capped with shorter chain thiols destabilized and aggregated in solution. To confirm that this destabilization was the result of ligand dissociating from the surface, excess ligand was added to the MPA and MHA solutions before the start of the 12 h reaction to ensure that the particle surface was saturated with ligands. In the presence of additional ligand, the particles showed no change in Z-average radii over the course of three days (Figure 3b). This indicated that the difference in stability between these three ligands came from the differences in their dissociation rates. Dissociation rates for ligands on CdSe were measured for amines ligands in organic solvents and were found to be 0.01 s^{-1}.[37] Our results for the C3 and C6 ligands indicate similar rates of dissociation, while the rate of dissociation for the C11 ligand is likely much slower given the stability of these particles.

In the case of the shortest chain ligand MPA, the excess ligand stabilized the colloid solution at an intermediate stage of aggregation. In this intermediate aggregation

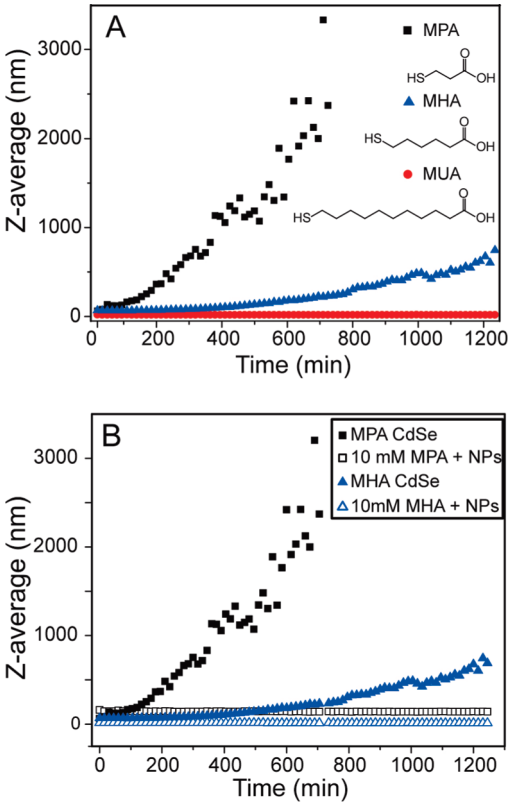

Figure 3. Aggregation behaviors for 4.1 nm CdSe nanocrystals as a function of chain length. (A) The measured Z-average for each of the capping agents as a function of time, indicating the decreased stability of shorter chain ligands on the surface of CdSe nanoparticles. (B) Stability test of MPA and MHA capped particles with excess ligand added to the solution. The addition of excess ligand (10 mM) to the solution of 7×10^{-7} M CdSe particles radically changes the stability of the solutions, inhibiting aggregation over the 12 h experiment.

state, the stabilized hydrodynamic radius of the MPA particles was 114 nm (Figure 3b), much greater than the 6−9 nm expected for a single particle with a 4.1 nm core. The larger hydrodynamic radius arises from aggregates which contain tens of particles that are able to participate in reversible binding, indicating that rapid ligand exchange and the presence of excess organic matter can lead to reversible aggregation. This behavior was not seen in particles capped with longer chain ligands, which maintained hydrodynamic radii between 7 and 10 nm.

The effect of ligand instability was quantified for these particles as a function of ionic strength. The CCC as a function of the aliphatic chain length changed dramatically for each of these ligands (Figure 4). Particles stabilized with shorter aliphatic chains were less stable than those capped with the longer chain ligands. The initial zeta-potential measurements (Table 1) indicated very similar surface charge densities for all of these particles. In order for aggregation to occur, charge neutralization must proceed by one of two mechanisms: (1) screening of the dielectric layer around the particles and (2) dissociation of the charged ligand from the surface. If screening of the dielectric layer were the predominate mechanism for destabilization, then zeta-potential measurements would predict similar CCCs for each of these coatings. Given the wide range of observed CCCs, the ligand dissociation

(50) Wiley, B.; Sun, Y. G.; Xia, Y. *Acc. Chem. Res.* **2007**, *40*, 1067–1076.
(51) Yin, Y. D.; Erdonmez, C.; Aloni, S.; Alivisatos, A. P. *J. Am. Chem. Soc.* **2006**, *128*, 12671–12673.

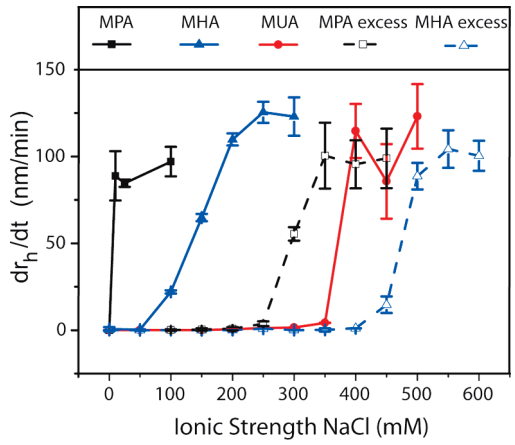

Figure 4. Plot showing the relationship between the aggregation rate and ionic strength for each of the capping ligands, which demonstrates the increased stability of ligands with longer aliphatic spacers.

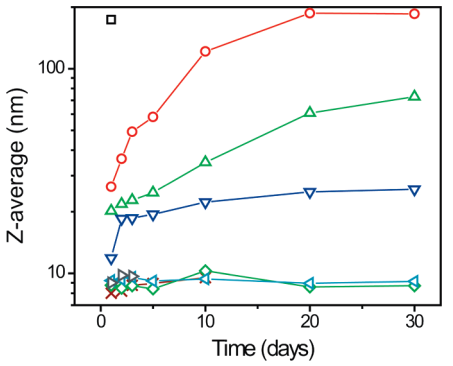

Figure 5. Stability of MUA capped particles as a function of pH. In basic solutions, 4.1 nm CdSe suspensions are stable for at least 30 days, without significant aggregation. Black squares, pH 4.24; red circles, pH 4.88; green triangles, pH 5.30; blue inverted triangles, pH 6.60; red ×, pH 8.70; green diamonds, pH 9.61; left green triangles, pH 10.92; brown right triangles, pH 12.02.

mechanism must have a significant role in the destabilization and aggregation of these solutions. Further evidence for ligand exchange in nanoparticle suspensions stabilized with MPA and MHA is seen in NMR spectra (Supporting Information, Figure S4), where narrow peaks and the thiol methylene resonance at 2.25 ppm both indicate the presence of free ligand in these nanoparticle solutions.

The addition of excess ligand dramatically changed the CCC for the MPA and MHA capped particles. The CCC for both the MPA and MHA coated particles increased and became comparable to the CCC for the MUA capped particles. In the presence of excess ligand, the surface charge of the MPA and MHA particles was stabilized, making charge screening the dominant mechanism for aggregation. Interestingly, the CCC of the MHA particles with excess ligand exceeded the CCC of the MUA particles. The excess MHA in solution insures the best possible surface coverage, possibly explaining the enhanced stabilization. The equivalent experiment with excess MUA is complicated by the presence of large MUA micelles which scatter light very strongly, inhibiting the collection of accurate DLS data.

For the most stable ligand, MUA, particle aggregation was monitored as a function of pH (Figure 5). Solutions were prepared by adjusting the initial pH with small amounts of NaOH or HCl. Monitoring of the hydrodynamic size took place over the course of 30 days and revealed the importance of pH for the stabilization of the ligand shell. In acidic solutions, near the pK_a of the carboxylic acid (4.9), the rate of aggregation was very high due to a decrease in zeta potential after protonation of the acid (see Supporting Information, Figure S6). At pH values above the pK_a of the carboxylic acid, but less than 8.7, protonation of the particle thiolate bonds (pK_a = 10.5) is favorable and played a significant role in particle destabilization. In basic solutions (pH > 8.7), MUA capped particles remained stable for at least 30 days without any sign of aggregation. Interestingly, the stable cluster size also behaved as a function of pH, where lower pH values drove the equilibrium toward greater degrees of aggregation. This trend was consistent with the earlier observations with the shorter chain ligands where ligand dissociation in the case of MPA led to stable cluster sizes larger than the hydrodynamic radius of single particles.

Nanoparticle/ligand interactions are often incorrectly thought to be static. The dynamic nature of these interactions makes nanoparticle stability quite sensitive to the solution composition. Even small changes in the surface coating have been shown to significantly change nanoparticle stability as a result of both primary particle/ligand interactions and secondary ligand/ligand interactions. In the case of short chain ligands, dissociation has been shown to be a primary mechanism for nanoparticle aggregation. When longer chain capping agents are used, the stability of the nanoparticle/ligand interaction increases, making charge screening the dominant destabilization mechanism.

Size and Shape Effects. Quantitative relationships between size and stability are important for understanding the potential risk of nanoparticles in the environment. Size dependent chemical and physical properties for CdSe have been reported[5,6] including a recent review[52] which indicated that factors such as size, shape, surface coating, and stability all influence the toxicity of CdSe nanoparticles. Peng and co-workers have shown that for small CdSe particles the stability of the particles was related to size because of changes in the electronic structure of the nanoparticles.[31] They concluded that the bond strength between the NP and thiolate was stronger for smaller particles because of increased overlap between the bonding orbital on the sulfur and the conduction band of the CdSe. Their results presupposed that ligand dissociation rather then charge screening was the dominant destabilization mechanism. This is likely true for the short chain ligands used in their study, but this explanation alone does not adequately predict the behavior of larger ligands, such as MUA. In order to determine the effect of size and shape on screening dominated destabilization, we used MUA capped particles, which experience very little ligand dissociation even after 30 days at pH 10 (Figure 5).

(52) Hardman, R. *Environ. Health Perspect.* **2006**, *114*, 165–172.

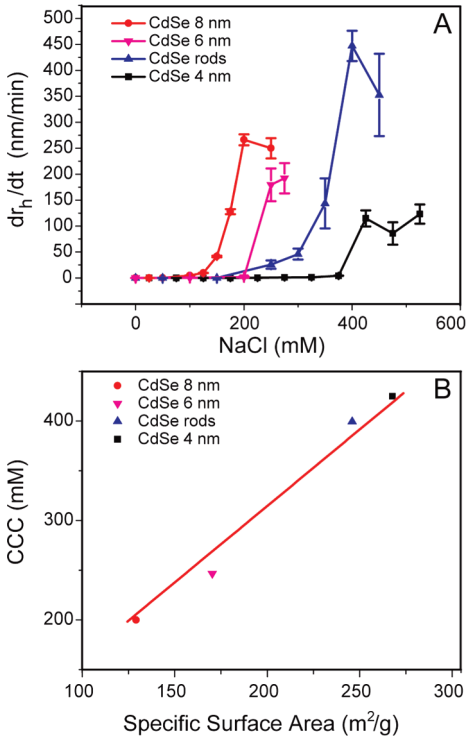

Figure 6. Nanoparticle stability as a function of size and shape. (A) The aggregation rate as a function of salt concentration for each of the nanoparticle samples. (B) A plot of the CCC as a function of the specific surface area, with the best fit line, assuming an intercept of 0. There is very good agreement with the data; $R^2 > 0.99$.

The CCC was determined for solutions of 4.1, 5.8, and 7.8 nm spheres, along with rods which were 2.9 × 24 nm. The 4 nm particles were the most stable and had a CCC of 425 mM NaCl, while the larger 8 nm nanocrystals aggregated in lower ionic strength solutions with a CCC of 200 mM NaCl (Figure 6a). As expected, the $(k_{11})_{diff}$ increased with increasing hydrodynamic radius of the particles. Interestingly, the CCC did not follow the same trend. The rods, which had a much larger hydrodynamic radius (32 nm), had a CCC between the 4 and 6 nm spheres. In addition to different particles sizes, there were also different surface areas for each of these samples. When the CCC was expressed as a function of the specific surface area (m^2/g), then a simple trend emerged (Figure 6b). For the range of particles examined, the CCC follows the expression CCC = 1.54*a*, where *a* is the specific surface area expressed as m^2/g.

According to DLVO theory, the stabilization of charged colloids has been shown to be a function of two opposing forces: electrostatic repulsion and van der Waals attraction.[41,42] The zeta-potential measurements showed that for each particle type the surface charge density was the same. Consequently, the electrostatic stabilization potential for each particle will be a function of the surface area. The linear dependence on surface area will therefore be expected for classes of nanoparticles with the same composition because the attractive van der Waals force will depend solely on particle morphology. Further work is currently underway to determine the limits of this linear relationship and to understand what role changing the nanoparticle material will have on this relationship.

Conclusions

Ligand design influences the kinetic stability of these nanoparticles. We have shown that in addition to binding strength, secondary factors, such as chain length, play an important role. Additionally, we have shown that for kinetically stable systems (minimal ligand exchange) that the most important factor in predicting stability is the surface area of the particles. The relationship between the surface area and particle stability provides a practical way to estimate the stability of nanoparticles using a readily measurable quantity. These general relationships will be useful references for material scientists to create more environmentally friendly nanomaterials and for environmental scientists to predict the fate and transport of nanoparticles.

Acknowledgment. This work was carried out under U.S. Department of Energy contract number DE-AC03-76SF-00098. Funding was provided by the U.S. Department of Energy, the joint BER-EPA-NSF nanoparticulate research program. Work at the Molecular Foundry was supported by the Office of Science, Office of Basic Energy Sciences, of the U.S. Department of Energy under contract number DE-AC02-05CH11231. We thank Dr. Emory Chan for the synthesis of nanoparticles.

Supporting Information Available: Additional information, as noted in the text, including kinetic plots and ATR-IR data, and additional NMR data. This material is available free of charge via the Internet at http://pubs.acs.org.